
Article:
Shui, W., Zhou, M., Maddock, S. orcid.org/0000-0003-3179-0263 et al. (6 more authors) (2020) A computerized craniofacial reconstruction method for an unidentified skull based on statistical shape models. Multimedia Tools and Applications, 79. pp. 25589-25611. ISSN 1380-7501

https://doi.org/10.1007/s11042-020-09189-7

A Computerized Craniofacial Reconstruction Method for an Unidentified Skull based on Statistical Shape Models

Wuyang Shui[1*], Mingquan Zhou[1], Steve Maddock[2], Yuan Ji[3], Qingqiong Deng[1], Kang Li[4], Yachun Fan[1], Yang Li[3], Xiujie Wu[5]

[1] School of Artificial Intelligence, Beijing Normal University, Beijing, 100875, China;

[2] Department of Computer Science, University of Sheffield, Sheffield, S10 2TN, UK;

[3] Institute of Forensic Science, Ministry of Public Security, Beijing, 100038, China;

[4] College of Information Science and Technology, Northwest University, Xi'an, 710127, China;

[5] Key Laboratory of Vertebrate Evolution and Human Origins, Institute of Vertebrate Paleontology and Paleoanthropology, Chinese Academy of Sciences, Beijing 100044, China;

Abstract: Craniofacial reconstruction (CFR) has been widely used to produce the facial appearance of an unidentified skull in the realm of forensic sciences. Many studies have indicated that the computerized CFR approach is fast, flexible, consistent and objective in comparison to the traditional manual CFR approach. This paper presents a computerized CFR system called CFRTools, which features a CFR method based on a statistical shape model (SSM) of living human head models. Given an unidentified skull, a geometrically-similar template skull is chosen as a template, and a non-registration method is used to improve the accuracy of the construction of dense corresponding vertices through the alignment of the template and the unidentified skull. Generalized Procrustes analysis (GPA) and principal component analysis (PCA) are carried out to construct the skull and face SSMs. The sex of the unidentified skull is then predicted based on skull SSM and centroid size, rather than geometric measurements based on anatomical landmarks. Furthermore, a craniofacial morphological relationship which is learnt from the principal component (PC) scores of the skull and face dataset is used to produce a possible reconstructed face. Finally, multiple possible reconstructed faces for the same skull can further be recreated based on adjusting the PC coefficients. The experimental results show that the average rate of sex classification is 97.14% and the reconstructed face of the unidentified skull can be produced. In addition, experts' understanding and experience can be harnessed in production of face variations for the same skull, which can further be used as a reference for portraiture creation.

Keywords: Computerized craniofacial reconstruction; Skull digitization; Skull registration; Sex classification; Facial shape editing

1. Introduction

Craniofacial reconstruction (CFR) is used to produce a likeness of the facial appearance of an unidentified skull. This method has been used to provide recognition and identification when forensic experts are confronted with a seriously decomposed cadaver [1-3], or to recreate the facial appearance of a historical figure from skeletal remains [4, 5]. Manual CFR approaches, such as the anthropometrical American method, the anatomical Russian method and the combination Manchester method, have been used to produce a physical face by moulding clay or plasticine onto a skull or its replica [6]. However, these manual approaches require significant forensic expertise and are time-consuming. These CFR results are inflexible and it remains a challenge for forensic experts to quickly produce a range of possible reconstructed faces of the unidentified skull.

Various computerized CFR approaches have been investigated with the aim of increasing objectivity, speed, efficiency and flexibility [7]. Miyasaka et al developed a 2D computer system based on image composition, which consisted of image processing and image editing units [8]. Suitable facial component images that conformed to a skull were selected and pasted over the initial facial framework. With the progress in computer graphics techniques, Vanezis et al developed a 3D computerized CFR system that combined skull digitization and computerized CFR [1, 9]. The 3D facial appearance profile of the unidentified skull was generated using facial soft-tissue thickness measurements (FSTMs) of every anatomical landmark of a template face. Particular organs (such as eyes, mouth and nose) could then be replaced to improve the accuracy of the CFR. Although FSTMs of various template faces can be used to produce multiple faces [10], this computerized CFR method does not provide an interactive face editing tool to allow a user to modify the 3D facial shape.

An alternative approach to use virtual sculpture software and haptic feedback techniques to create three-dimensional (3D) facial appearance, mimicking the traditional Manchester method [5, 7]. A digital skull is imported and tissue-depth pegs are attached to its surface at anatomical sites. Facial muscle models are interactively placed on the digital skull and then eyes, ears and a nose are chosen to integrate with the rough facial appearance. This approach has been widely used in the field of archaeology and forensic science; however, such a system still requires anatomical knowledge and modelling software skills.

Our work presents a pipeline for computerized CFR based on a statistical shape model (SSM). Our CFRTools system integrates tasks such as skull digitization, calculation of geometric measurements, sex classification, computerized CFR and facial shape editing. It can be used to assist forensic experts in quickly creating modifiable and flexible 3D facial appearances. The contributions of this paper are as follows:

1. A template skull and a non-rigid registration algorithm are used to improve the accuracy of skull registration and construct a high-quality set of dense corresponding vertices between the template skull and the unidentified skull;
2. Repeatable geometric measurements can be calculated on the digital skull based on a specific virtual plane and curve fitting methods, overcoming the drawbacks of traditional craniometry;
3. The skull SSM and centroid size are used to realize sex classification of the unidentified skulls, rather than a few geometric measurements;
4. Variations of the CFR results can flexibly be created based on a craniofacial morphological relationship learnt from principal component (PC) scores of the skull and face SSMs.

The rest of the paper is organized as follows. Section 2 presents related work. Sections 3 and 4 describe the materials and the computerized CFR methods we have used. Section 5 presents results. In section 6, we conclude the paper.

2. Related work

Many previous studies have described the advantages of computerized CFR approaches [1, 11, 12], however, manual 2D and 3D approaches continue to be used for both forensic purposes and archaeology [13]. One reason may be that only a few teams have access to a computerized CFR system, which requires sophisticated computer-based techniques and a database containing a large skull and face models dataset [14].

The computerized CFR result depends on the quality of the digital skull, which is usually generated by the non-contact measurement technique. Both laser scanning and CT have been used to obtain a digital skull [11, 15]. For a decomposed body, CT scanning is the preferred technique since bone models can easily be generated without resorting to skeletonization of the body. Typically, both the interior and exterior structures of the skull, facial soft-tissues and the U-shaped plates of the CT device can be digitized [12]. Laser scanning is an alternative choice when only the cranium and mandible are remaining. For example, a laser scanner and a camera have been used to acquire a digital skull for computerized CFR [1, 9]. In this procedure, multiple scans from different positions must be taken and then aligned to generate a complete digital skull using the Iterative closest point (ICP) registration algorithm [16]. Alternatively, to overcome registration error accumulation, a multi-view registration algorithm can be used to register all the scans simultaneously [17, 18]. A previous study compared geometric deviation of the models that were acquired by both laser scanning and CT scanning techniques, and it indicated that both techniques can be used to generate a high-quality digital skull [15].

A vital part of quantitative forensic investigation is to calculate geometric measurements on the unidentified skull, so as to recognize the geometric characteristics of the person [19]. However, traditional craniometry suffers from several drawbacks [20]. For example, it remains a challenge to accurately measure the distance between a landmark and the specific plane because this plane cannot easily be shown in relation to a physical skull. Also, it is problematic to measure the length of the boundary curve of a damaged bone. A useful tool needs to be developed to bring repeatability and objectivity to these measurements, which can be used to quantitatively compare shape difference between various skulls.

Determining sexual dimorphism from the human skull is a necessary step before computerized CFR [6, 21, 22]. Since male's skull is always larger than female and geometric surface of male's skull is much rougher, many studies have attempted to differentiate males and females based on experts' observation and experience [22]. However, high inter-observer errors might result in worse classification when forensic experts lack experience [23]. To address this problem, quantitative methods, for example discriminant function analysis and logistic regression analysis, have become popular [19, 24, 25]. Geometric measurements of every skull are calculated to represent the dimorphic characteristics of the skull. Then, the classifiers or discriminant equations are provided to predict the sex. The drawback of this method is that only a few measurements are typically used to represent the geometric shape of the skull. In addition, the extent to which the choice of measurements influences sex classification needs to be investigated.

In recent years, dense corresponding vertices have been used to investigate facial shape

difference and sexual dimorphism based on principal components (PCs) [21, 26]. Our previous work reported on experiments about sex classification of the face [27]. However, the extent to which the choice of PCs influences the sex classification rate of the skull needs further investigation. In geometric morphometrics, centroid size which is defined as the square root of distance between all the vertices and their centroid has been used to represent size factor of the specimen [28]. Although the relationship between centroid size and sex and age factors has been investigated, only a few studies have adopted this to realize sex classification. In this study, centroid size and shape will be used to enhance the accuracy of sexual dimorphism.

Because the effect of dense corresponding vertices among different models influences the quality of SSM, various rigid and non-rigid registration methods have been investigated. Example approaches include optical flow [29], generalized Procrustes analysis (GPA) and thin-plate spline (TPS) [21, 30], ICP and TPS [31], TPS and compactly supported radial basis functions (CSRBF) [12], TPS-RPM [32], and coherent point drift (CPD) [33]. In addition, the well-known non-rigid ICP (NICP) has been widely used to realize models registration and construct dense corresponding vertices of face models, guided by anatomical landmarks to ensure convergence [34-36]. In this procedure, registration loops were iteratively performed by decreasing stiffness weights and incrementally deforming the template. Booth et al. demonstrate NICP method enhances the effectiveness of the construction of dense corresponding vertices and shape reconstruction for the face models [37]. Because of the complex geometrical shape of skulls, it still remains a challenging to improve the accuracy of skull registration using NICP.

More recently, with the increasing number of skull and face model datasets that are derived from medical images, regression-based approaches have been used to realize computerized CFR [31, 38-41]. The basic principle of these methods is to apply the learnt craniofacial relationship to the unidentified skull. Principal component analysis (PCA) is employed to compute PC scores and corresponding PCs of every skull and face, and then the craniofacial relationship is learnt based on the regression of PC scores of skull and face datasets. Since the reconstructed face relies on the geometric shape of the skull, the craniofacial morphological relationship, as well as sex, age, body mass index, nutrition, etc., the reconstructed face is probably not the same as the actual face. An interactive face edit tool should be offered to assist users to refine the reconstructed face. Although previous studies have analyzed the variability of facial shape based on the face SSM [27, 42], the extent to which the choice of PCs revises the geometric shape of the reconstructed face needs careful consideration so as to produce a flexible process, as well as controllable and plausible results.

3. Materials

In this study, 140 living individuals (70 females and 70 males) of Han Chinese nationality were recruited to construct the skull and face dataset [12, 27]. Triangle meshes of the exterior surfaces of every skull and face were generated and positioned in the Frankfurt Horizontal coordinate system, respectively. Then, 78 anatomical landmarks and corresponding facial landmarks were interactively placed on every skull and face model, respectively. The rigid and non-rigid registration algorithms were used to register a template model (skull or face) with every target model (skull or face). Thus, dense corresponding vertices were constructed based on the assumption that the closest points between two models were corresponding, i.e., each corresponding vertex with the same index occupied the same relative position in every sample. In the following sections, every skull and face will be respectively denoted by $S=\{[x_{i,1}^S, y_{i,1}^S, z_{i,1}^S,...,x_{i,m}^S, y_{i,m}^S, z_{i,m}^S]^T, i=1,2,3,...,N;\}$ and

$F=\{[x_{i,1}^F, y_{i,1}^F, z_{i,1}^F,...,x_{i,n}^F, y_{i,n}^F, z_{i,n}^F]^T, i=1,2,3,...,N;\}$, where N, m, and n denote the number of samples within the dataset, the number of skull vertices, and the number of face vertices.

4. Methods

Fig. 1 summarizes the pipeline used in our computerized CFR method. The first step is digitization of the unidentified skull. Either CT images or laser scanning is used to generate a triangle mesh of the exterior surface of the unidentified skull. Second, geometric measurements are calculated on the digital skull. Example measurements include the lengths of the boundary curves of the orbit and nasal bone, and the distance between an anatomical landmark and a specific virtual plane. Third, a template skull is deformed to the unidentified skull using the hybrid non-rigid registration method. Dense corresponding vertices are constructed based on the assumption that the closest point is considered as the corresponding vertex. Fourth, sexual dimorphism is determined based on a two-class pattern classification. Support vector machines (SVMs) are used to construct a classifier to predict the sex based on PC scores and centroid size. Finally, the reconstructed face of the unidentified skull is produced based on a regression-based CFR method. A range of possible reconstructed faces can be further generated by adjusting the PC coefficients. More details will now be given on each of these stages.

4.1 Digitization of an unidentified skull

Before attempting computerized CFR, it is necessary to convert a physical skull to a digital model. Two approaches can be used, CT scanning or laser scanning, depending on the initial state of the physical skull, i.e. whether or not it is surrounded by soft tissue. There was no risk for skull damage during digitization procedures. For the CT scanning, the bone was segmented by setting a threshold and then the Marching Cubes algorithm was used to convert voxels to a set of triangle meshes [43]. Subsequently, the exterior surface of the unidentified skull was extracted using three steps. First, four skull landmarks, the left porion (*Lp*), the right porion (*Rp*), the left orbitale (*Lo*) and the glabella (*G*), were interactively placed on the skull and then the skull was transformed into the Frankfurt coordinate system. Second, a cylinder was defined which covered the digital skull. The exterior point cloud of the digital skull was extracted by computing the intersection points between the digital skull and rays, starting at each sampling point of the cylinder, denoted by $p_i(x_i, y_i, z_i)$ with orientation $(\frac{x_i}{\sqrt{x_i^2 + y_i^2}}, \frac{y_i}{\sqrt{x_i^2 + y_i^2}}, 0)$ [44]. Finally, the point cloud was converted to a triangle mesh.

For the laser scanning approach, five steps were used. First, the unidentified skull was placed on a turntable and multiple scans from different positions were acquired. Second, the classic 4-Points Congruent Sets (4PCS) algorithm was used to coarsely register overlapped scans by extracting all coplanar 4-points sets from a 3D point set and computing the affine transformation of every scan [45]. Third, a point-to-plane ICP algorithm was applied to register all the scans. Local shape descriptors (such as normal and curvature) and the distance of corresponding points were used to reject outliers and improve the accuracy of registration. Fourth, global positions were calculated and each scan was registered to these global positions, addressing the problem of accumulated errors when multiple scans were registered incrementally [46]. Finally, a fusion point cloud was converted to a triangle mesh.

4.2 Geometric measurements

Forensic experts may wish to calculate geometric measurements on the skull, for example, the distance from a landmark to a specific plane. To accurately and repeatedly measure this distance, experts can interactively place the landmarks on the skull and the specific plane can be further fitted and illustrated based on these marked landmarks. Assuming some landmarks are placed on the digital skull, denoted by $Q=\{q_1,q_2,\mathrm{L},q_k\}, q_i=(x_i,y_i,z_i)$ and the specific plane is represented by the equation $z=a_0x+a_1y+a_2$, the least square method can be used to compute the coefficients of the best-fitting plane by minimizing the following equation

$$\mathrm{E}=\min\sum_{i=0}^{k-1}\left\|\left(a_0x_i+a_1y_i+a_2-z_i\right)\right\|^2 \tag{1}$$

where a_0, a_1 and a_2 denote the coefficients of the fitted plane and k denotes the number of the landmarks.

Forensic experts may also require to measure the length of the boundary curve on certain notable skull structures, for example, the lengths of the boundary curves of an orbit or the nasal bone. The boundary vertices of the orbit are extracted from the exterior triangle mesh of the skull based on the assumption that the one-ring adjacent points of every boundary vertex do not for a close loop. Then, the bounding box of the orbital outline, as well as its width and height can be computed. The length of the boundary curve is calculated as the sum of the line segments between neighbouring vertices. Also, these boundary curves will be used to guide skull registration. In addition, the damaged bone often results in errors in the calculation. To address this problem, the boundary vertices of missing regions are extracted and deBoor's algorithm [47] is applied to virtually repair the incomplete curve by fitting a B-spline curve.

4.3 Alignment of the unidentified skull

The selection of the template skull will impact on the accuracy of skull registration as well as the construction of dense corresponding vertices. The most similar skull is selected in relation to geometric shape from a skull dataset as the template model. Based on the definition of anatomical landmarks on the skull [48], we firstly placed 78 landmarks on the unidentified skull, denoted by $Qskull$. Then, the ICP algorithm was applied to rigidly deform $Qskull$ to every skull within our skull dataset. Finally, the quantitative distance of each vertex between $Qskull$ and the closest point on every skull within the skull dataset can be calculated and depicted in a graphical format using a colour bar. This procedure can repeat and the average error (*avergskullError*) is calculated by computing the average value of quantitative distances of all the vertices on $Qskull$. The skull within the dataset which has the smallest average error is chosen as the template.

After the template skull is selected and represented by $template=(\mathrm{V},\varepsilon)$, where V denotes a set of vertices and ε denotes a set of edges, the hybrid registration algorithm was implemented to improve the accuracy of skull registration. The ICP algorithm was firstly used to rigidly deform $template$ to $Qskull$, eliminating shape differences in position and orientation. Then, the NICP algorithm was used to deform the template skull to $Qskull$ by assigning an affine transformation to each vertex and minimising the difference in the transformation of neighbouring vertices [34]. In this procedure, both manually placed landmarks and the calculated boundary landmarks are used to guide registration. Finally, dense corresponding vertices between two skulls can be constructed.

Following the registration framework of NICP, an affine transformation $\mathbf{X}_i$ can be defined on

each vertex of *template* with all these transformations can be defined as $\mathbf{X} = [\mathrm{X}_1\mathrm{X}_2\mathrm{X}_3\cdots\mathrm{X}_n]^{\mathrm{T}}$. A local affine regularisation term, $E_{\mathrm{d}}(\mathbf{X})$, a stiffness term, $E_s(\mathbf{X})$, a skull landmarks term, $E_l(\mathbf{X})$, and a boundary curve term, $E_b(\mathbf{X})$, are used to define the weighting cost function

$$E(\mathbf{X}) = E_{\mathrm{d}}(\mathbf{X}) + \alpha E_l(\mathbf{X}) + \beta E_s(\mathbf{X}) + \lambda E_b(\mathbf{X}) \tag{2}$$

where α denotes the weighting of anatomical landmarks, β denotes the stiffness weighting that balances the importance of each term, and λ denotes the weighting of corresponding vertices of boundary curves .

The local affine regularization term expresses the distance between a vertex of *Qskull* and the corresponding vertex on the *template*

$$E_{\mathrm{d}}(\mathbf{X}) = \sum_{v_i \in v} \varpi_i dist^2(Qskull, X_i v_i) \tag{3}$$

where ϖ_i denotes the reliability of correspondences between *Qskull* and *template* . A kd-tree was used to speed up nearest point searching and the closest point was taken as the corresponding vertex. Normal orientation and the distance between corresponding vertices, were used to reject outliers and guarantee the accuracy of correspondences.

The stiffness term is applied to regularize the deformation

$$E_s(\mathbf{X}) = \sum_{(i,j)\in\varepsilon} \left\| (X_i - X_j)\cdot G \right\|_F^2 \tag{4}$$

where $\|\cdot\|_F$ denotes the Frobenius norm and $G = diag(1,1,1,\gamma)$ denotes a weighting matrix.

The anatomical landmarks term is used to initialize and guide registration

$$E_l(\mathbf{X}) = \sum \left\| X_i v_i - m_i \right\|^2 \tag{5}$$

where m_i is the *i*-th anatomical landmark of *Qskull* and v_i is the corresponding *i*-th anatomical landmark of *template* .

The boundary curve term is used to initialize and guide registration

$$E_b(\mathbf{X}) = \sum \left\| X_i v\mathrm{Edge}_{k,\ i} - m\mathrm{Edge}_{k,\ i} \right\|^2 \tag{6}$$

where $m\mathrm{Edge}_{k,\ i}$ represents the *i*-th vertex of the *k*-th boundary curve of *Qskull* and $v\mathrm{Edge}_{k,\ i}$ represents the corresponding *i*-th vertex of the corresponding *k*-th boundary curve of the template skull.

Two skulls were often well registered after the geometrically-similar skull was selected and the NICP algorithm was implemented. To quantitatively evaluate the accuracy of skull registration, the quantitative distance of each vertex between *Qskull* and the closest point on the *template* can be calculated and depicted in a graphical format. This procedure can repeat and the average error (*avergError*) can be calculated by computing the average value of quantitative distances of all the vertices on *Qskull* .

4.4 Sexual dimorphism

This study presents a sexual dimorphism algorithm for the skull based on the SSM and centroid size, which draws inspiration from previous work in relation to face SSM [27, 28] . It contains two stages: a training stage and a test stage. In the training stage, PC scores and centroid size were used

to represented the shape and size of every skull. The centroid size of every skull was calculated by computing the sum of the distances between every vertex and the centroid. Then, GPA and PCA were applied to dense corresponding vertices of every skull, removing translation, rotation and scaling factors[49]. Therefore, every skull was represented by the coordinates of the average skull, the linear combinations of PC scores and corresponding orthogonal PCs. Based on the sex label, these PC scores and centroid size of every skull, SVMs were used to construct a sexual dimorphism classifier by searching for a linear separating hyperplane with maximal margin.

In the test stage, landmarks were manually placed on *Qskull* and dense corresponding vertices of *Qskull* were constructed after skull registration was performed. PC scores and centroid size of the *Qskull* were calculated, respectively, which are then input to the sexual dimorphism classifier. In this study, we used LIBSVM to create SVMs to realize sexual dimorphism [50].

4.5 Computerized CFR

4.5.1 Computerized CFR by linear regression

The quality of the learnt craniofacial relationship impacts on the accuracy of computerized CFR. Unlike previous work [27], GPA and PCA were carried out to construct a skull and face SSM, respectively. Then, every skull was represented by $(\overline{\mathbf{averskull}}, \mathbf{SkullCoeff}, \mathbf{sv})$, where $\overline{\mathbf{averskull}}$ denotes the average skull, $\mathbf{SkullCoeff} = [\boldsymbol{\alpha}_{1,d}, \boldsymbol{\alpha}_{2,d}, \cdots, \boldsymbol{\alpha}_{N,d}]$ denotes PC scores and $\mathbf{sv} = [\mathbf{sv}_1, \mathbf{sv}_2, \mathrm{L}\ , \mathbf{sv}_d]$ denotes corresponding PCs. Also, every face can be represented by $(\overline{\mathbf{averface}}, \mathbf{FaceCoeff}, \mathbf{sw})$, where $\overline{\mathbf{averface}}$ denotes the average face, and $\mathbf{FaceCoeff} = [\mathbf{b}_{1,f}, \mathbf{b}_{2,f}, \cdots, \mathbf{b}_{N,f}]$ denotes PC scores and $\mathbf{sw} = [\mathbf{sw}_1, \mathbf{sw}_2, \cdots, \mathbf{sw}_f]$ denotes corresponding PCs. Finally, the craniofacial relationship, $\mathbf{M}$, related to our dataset was quantitatively computed by a partial least square regression (PLSR) [41].

After the dense corresponding vertices of the unidentified skull were constructed by the non-rigid registration method, we used GPA and PCA to calculate the PC scores of *Qskull* , denoted by $\mathbf{Qskull\alpha}$. Then, PC coefficients of the reconstructed face, denoted by $\mathbf{Qface\alpha}$, were computed using the following equation $\mathbf{Qface\alpha} = \mathbf{Qskull\alpha} \cdot \mathbf{M}$ .The reconstructed face was further computed by

$$\mathbf{FaceVector(Qface\alpha)} = \overline{\mathbf{averface}} + \sum_{i=1}^{f} Qfacea_i \cdot \mathbf{sw}_i \tag{7}$$

where $\mathbf{Qface\alpha} = [Qfacea_1, Qfacea_2, ..., Qfacea_f]$, $Qfacea_i$ denotes the *i*-th PC coefficient of the reconstructed face and *f* denotes the number of PCs.

To quantitatively evaluate the accuracy of CFR, the quantitative deviation of each vertex between the reconstructed face and the actual face produced by the average face and a linear combination of PC scores and PCs was calculated and depicted in a graphical format. This procedure can repeat and the average error (*reconstructionError*) of quantitative deviations of all the vertices of every sample was calculated.

4.5.2 Facial appearance editing

This study examined the effect of each PC related to face variation in the face SSM by comparing the geometric shape of the average face and the new face, denoted by $\mathbf{FaceNew}$. The new face was generated by adjusting the PC coefficient of every PC

$$\mathbf{FaceNew}(\lambda) = \overline{\mathbf{averface}} + 3\lambda \cdot \delta_i \cdot \mathbf{sw}_i \quad (8)$$

where δ_i denotes standard deviation of the *i*-th PC and the weighting coefficient λ is set to -1.0 and 1.0.

Previous work added the eigenfaces to the average face to produce a new face [51, 52]. Using this idea in our system, experts can interactively adjust the PC coefficients, denoted by $\boldsymbol{\varphi} = \{\varphi_i\}$, of every PC to present a range of possible reconstructed faces. Variations of the same face can be created by the following

$$\mathbf{FaceNew}(\boldsymbol{\varphi}) = \overline{\mathbf{averface}} + \sum_{i=1}^{f} \varphi_i \mathbf{sw}_i \quad (9)$$

In addition, the eyes, nose, and mouth of $\mathbf{FaceNew}(\boldsymbol{\varphi})$ can be replaced using the technique from previous work[53]. The organs of the reconstructed face can be interactively removed. More appropriate eyes, nose and mouth can be selected from organ datasets based on the experts' experience and knowledge. These selected organs are then registered to **FaceNew**, making these components tightly match **FaceNew**.

5. Experimental Results

5.1 Skull digitization

Both CT scanning and laser scanning technologies were used to digitize the unidentified skull. In a real forensic case, CT scanning is the preferred technique to generate the exterior surface of the unidentified skull. The main reason is that the digital skull can be produced without resorting to skeletonization. All the data can then be immediately and electronically sent, saving operational time. Another reason is that both exterior and interior structures, as well as the fracture surface of a damaged skull can be generated and archived. Fig. 2 shows an example of a digitized skull based on CT images. Fig. 2a shows the CT images of the unidentified skull, which consists of 510 images. A threshold was used to segment bone from the CT images and the Marching Cubes algorithm was used to convert the voxels to the digital skull (Fig.2b). Figs. 2c and 2d show the exterior point cloud and the exterior surface of the unidentified skull, respectively.

A Konica Minolta VIVID 910 laser scanner was used to acquire another unidentified skull. Fig. 3a shows the unidentified skull placed on a turntable and twelve scans were acquired from various positions. Figs 3b and 3c show an example of two neighbouring scans which are located in a common coordinate system and the coarse registration result via the 4PCS algorithm, respectively. As seen in the Fig. 3c (in the rectangle), there were registration errors around the nasal bone. The fine registration result was obtained via the ICP algorithm considering outlier rejection (Fig.3d). Fig. 3e shows the result of registering multiple scans using global positions. This global registration method has a better registration result.

5.2 Geometric measurements

This study offers repeatability and objectivity when calculating geometric measurements, which assists experts to conduct investigations. Fig. 4 shows the Euclidean distance between the landmark and the specific plane that was fitted based on at least three anatomical landmarks. Both the landmark and specific plane are illustrated on the digital skull as a reference. Fig. 4a shows the Euclidean distance (4.56 cm) between an anatomical landmark (the glabella) and the Frankfurt plane, which was generated using three landmarks. Fig. 4b shows the distance (4.48 cm) between another

anatomical landmark (the gonion) and the sagittal plane, which was fitted using six anatomical landmarks.

Fig. 5 shows the process of orbit detection from the exterior triangle mesh of the digital skull. Fig. 5a shows all the boundary curves (green points) of the digital skull and Fig. 5b shows the boundary curve of the right orbit, comprised of 75 vertices (green points). The length of the boundary curve of the orbit was 13.0 cm. Fig. 6a shows the boundary curve of the nasal bone. Missing regions led to an incorrect calculation of the length of boundary curve. Thus, six points located at the start and end of the missing regions were interactively placed on the boundary curve in a clockwise direction (Fig. 6b). Corresponding boundary vertices of missing regions (red points) are illustrated in Fig. 6c. Fig. 6d shows the repair of the damaged boundary curve using deBoor's algorithm. The length of the repaired boundary curve (green points) was 11.69 cm, which was calculated by summing the length of every line segment between neighbouring sample points. In comparison to existing work [20, 54], our method can repeatedly and accurately measure the length of the boundary curve of the damaged skull. These measurements are very helpful to analyse the geometric shape of the skull.

5.3 skull registration

The geometric shape of the skull is complex, and contains holes and thin-shell areas. An inappropriate template model that greatly differs from the unidentified skull leads to weak registration. In our work, we computed the geometric shape difference between the unidentified skull and every skull within the skull dataset, and then the most similar skull in shape was selected as the template model to improve the accuracy of skull registration. Fig. 7. shows the front and profile views of the unidentified skull (grey colour) and two candidate skulls (skin colour), where Figs. 7a, 7b and 7c show the unidentified skull (022), the candidate skull (023) and another candidate skull (1231), respectively. Fig. 8a shows the 023 skull (skin colour) as the template model is rigidly registered to 022 skull (grey colour). The quantitative distance of each vertex is depicted on the unidentified skull, where *avergskullError* is 3.63 mm. Fig. 8b shows No.1231 skull (skin colour) as the template model which is rigidly registered to 022 skull (grey colour). The quantitative distance of each vertex is depicted on the unidentified skull, where *avergskullError* is 3.51 mm. Because *avergskullError* of No. 1231 skull is much smaller, it would be chosen as the template model.

The corresponding vertices located at the boundary curves of every skull are used to register skulls. Similar to other work [55], eight boundary curves in total can be implemented, as illustrated in Fig. 9. To validate the effectiveness of the selection of the template, we used the ICP and NICP to deform two models to the unidentified skull. Fig. 10a shows the results that the most similar skull (1231) as the template model deformed to the unidentified skull (022), where *avergError* is 0.28 mm. Fig. 10b shows the results that No.023 skull as the template model deformed to No.022 skull, where *avergError i*s 0.34 mm. To evaluate the effectiveness of the registration algorithm, we compared with ICP and TPS method [31] and TPS and CSRBF method [12]. Fig. 11a shows the registration result between No.1231 and 022 skulls using ICP and TPS method, where *avergError i*s 1.04 mm. Fig. 11b shows the registration result between the same two skulls using TPS and CSRBF method, where *avergError i*s 1.01 mm. These results indicate that the selection of template and NICP can enhance the accuracy of skull registration.

Additionally, the non-rigid registration method can also be used to realize a damaged skull completion (Fig.12). From left to right, each figure respectively shows the registration result, the

registration result (skin colour) and the damaged skull (grey colour) in the common coordinate system, and the registration errors from the front and profile views. Fig. 12a shows the virtual restoration result of the damaged skull using our method. The quantitative distance of each vertex is depicted in a graphical format, where *avergError* is 0.46 mm. The TPS and CSRBF method [12] was used to deform the template skull to the damaged skull, where *avergError* is 1.35 mm (Fig. 12b).

5.4 Sex classification

After skull registration, dense corresponding vertices can be constructed based on the assumption that the closest point is equal to the corresponding vertex. GPA and PCA methods were applied to construct skull SSM, and then PC scores and centroid size of every skull as well as sex label were used to train the sexual dimorphism classifier. The sex label of every skull was set to 1 (male) or -1 (female) and SVMs with a radial basis function (RBF) kernel were applied to learn the relationship between the class labels and PC scores. We applied 5-fold cross-validation to evaluate the accuracy of the sexual dimorphism. All the skulls were randomly divided into five groups, where each group consisted of 50% males and 50% females. A classifier was then constructed based on four groups, and each skull of the remaining group was used as a test sample. Fig. 13 shows the sex classification rate in relation to the various number of PCs. It can be seen that the highest sex classification accuracy using our method was 97.14% and the highest sex classification accuracy using only PC scores was 95.71%. Our method compared with the use of Fisher discriminant analysis and PC scores of anatomical landmarks (the rate is 91.3% for males and 90.1% females) [56], and sexual discriminant equations (the rate is 87.4%)[57]. These results indicate that our method has a higher accuracy of sex classification.

5.5 Craniofacial reconstruction

Since the sex plays a significant role in the CFR, we realized CFR using PLSR in male and female groups, respectively. To validate the effectiveness of our method, 60 samples in each group were used as the training data to learn the craniofacial morphological relationship and the remaining 10 samples were chosen as test data. Fig. 14a shows the *reconstructionError* of every sample in the training data, where the average value of *reconstructionError* of the female group is 1.26 mm and the average value of *reconstructionError* of the male group is 1.19 mm. In comparison to the use of skull and face SSMs with size and least square approach [27], the average error value of our method which employed GPA, PCA and PLSR is smaller. It indicates that our method can learn more accurate craniofacial morphological relationship from training data. Fig. 14b shows the *reconstructionError* of every test sample, where the average value of *reconstructionError* of the female group is 3.39 mm and the average error value of *reconstructionError* of the male group is 3.82 mm. In comparison to the use of skull and face SSMs with size and the least squares method [27], the average error value in our method is smaller. It indicates that our method can produce a better reconstructed face. The geometric deviations of every vertex between the reconstructed face and the actual face for female and male groups in the training data are shown in Fig. 15, respectively. It can be seen that the geometric shape is great difference around the face cheek, forehead, neck, ears, etc.

The interactive edit can be further used to improve the accuracy of CFR. The face SSM was constructed to investigate the effect of each PC on the face variation of all the samples. Fig. 16

shows the facial shape variation related to the first four PCs using Eq. 8, where PC*i*+ denotes $\lambda = 1.0$ and PC*i*- denotes $\lambda = -1.0$. Each PC reflects a different morphological variation in the face. A comparison of the PC1+ and PC1- reveals that a decrease in the PC1 score is greatly related to a broadening of the cheek, chin and neck. A decrease in the PC2 score seems to explain the widening of cheek and a sloped forehead. Similarly, we can investigate the effect of every PC on the face variation of male and female groups, respectively. Fig. 17 shows an example of computerized CFR for the damaged skull with missing teeth (Fig.2). Figs. 17a and 17b, respectively, show the skull and the reconstructed face using our method. Our approach provides an interactive tool which allows users to create variations of the same face by adjusting PC coefficients. This allows them to use their understanding and experience to choose the appropriate facial appearance. Fig. 17c shows the edited face that was recreated by adjusting the PC coefficients of both PC1 and PC2. The geometric difference between the reconstructed face and the edited face is depicted in Figs. 17d and e. It can be seen that the cheek and neck of the edited face, as well as the back of the reconstructed face become greatly narrower.

6. Conclusion

In this paper, a computerized CFR method has been proposed based on skull and face SSMs of living humans. The CFRTools system supports computerized CFR. Our approach integrates a set of sophisticated tasks, including skull digitization, geometric measurements, sex classification and computerized CFR. Either experts or non-specialists can create a likeness of 3D facial appearance for an unidentified skull. After the exterior surface of the unidentified skull is extracted, our method constructs dense corresponding vertices of the unidentified skull based on a choice of template skull and the use of the NICP algorithm. Repeatable geometric measurements can be calculated on the digital skull based on a specific virtual plane and curve fitting methods. A sexual dimorphism classifier can be used to realize sex classification of the unidentified skull based on PC scores and centroid size. Finally, the learnt craniofacial morphological relationship is applied to the unidentified skull to produce a likeness of 3D facial appearance, which can be further edited by adjusting PC coefficients. Our future work will collect more skull and face models of living humans, and further improve the accuracy of computerized CFR considering the predicted age and face attribute (slim, normal or obese) of the person.

References

[1] Vanezis P, Blowes R, Linney A, Tan A, Richards R, Neave R (1989) Application of 3-D computer graphics for facial reconstruction and comparison with sculpting techniques. Forensic Sci Int 42(1-2), 69-84.

[2] Quatrehomme G, Cotin S, Subsol G, Delingette H., Garidel Y, Grévin G., Fidrich M, Bailet P, Ollier A (1997) A fully three-dimensional method for facial reconstruction based on deformable models. J Forensic Sci 42(4), 649-652.

[3] Wilkinson CM (2004) Forensic facial reconstruction. Cambridge University Press.

[4] Benazzi S, Fantini M, Crescenzio FD, Mallegni G, Mallegni F, Persiani F, Gruppioni G (2009) The face of the poet Dante Alighieri reconstructed by virtual modelling and forensic anthropology techniques. J Archaeol Sci 36(2), 278-283.

[5] Lee WJ, Yoon AY, Mi KS, Wilkinson CM, Dong HS (2014). The archaeological contribution of forensic craniofacial reconstruction to a portrait drawing of a Korean historical figure. J Archaeol Sci 49, 228-236.

[6] Wilkinson CM (2010) Facial reconstruction—anatomical art or artistic anatomy?. J Anat 216, 235-250.
[7] Wilkinson CM, Rynn C, Peters H, Taister M, Kau CH, Richmond S (2006) A blind accuracy assessment of computer-modeled forensic facial reconstruction using computed tomography data from live subjects. Forensic Sci Med Pathol 2, 179-187.
[8] Miyasaka S, Yoshino M, Imaizumi K, Seta S (1995) The computer-aided facial reconstruction system. Forensic Sci Int 74(1-2), 155-165.
[9] Vanezis P, Vanezis M, McCombe G, Niblett T (2000) Facial reconstruction using 3-D computer graphics. Forensic Sci Int 108(2), 81-95.
[10] Starbuck JM, Ward RE (2007) The affect of tissue depth variation on craniofacial reconstructions. Forensic Sci Int 172,130-136
[11] Claes P, Vandermeulen D, De Greef S, Willems G, Clement JG, Suetens P (2010) Computerized craniofacial reconstruction: Conceptual framework and review. Forensic Sci Int 201,138-145.
[12] Deng Q, Zhou M, Shui W, Wu Z, Ji Y, Bai R (2011) A novel skull registration based on global and local deformations for craniofacial reconstruction. Forensic Sci Int 208(1-3), 95-102.
[13] Hayes S (2016) Faces in the museum: revising the methods of facial reconstructions. Museum Management and Curatorship 31, 218-245.
[14] Quatrehomme G, Balaguer T, Staccini P, Alunni-Perret V (2007) Assessment of the accuracy of three-dimensional manual craniofacial reconstruction: a series of 25 controlled cases. INT J Legal Med 121(6), 469-475.
[15] Shui W, Zhou M, Chen S, Pan Z, Deng Q, Yao Y, Pan H, He T, Wang X (2017) The production of digital and printed resources from multiple modalities using visualization and three-dimensional printing techniques. INT J Comput Ass Rad 12, 13-23.
[16] Rusinkiewicz S, Levoy M (2001) Efficient variants of the ICP algorithm. Third International Conference on 3D Digital Imaging and Modeling, 145-152.
[17] Brown BJ, Toler-Franklin C, Nehab D, Burns M, Dobkin D, Vlachopoulos A, Doumas C, Rusinkiewicz S, Weyrich T (2008) A system for high-volume acquisition and matching of fresco fragments: Reassembling Theran wall paintings. ACM T Graphic 27(3): No.84.
[18] Tang Y, Feng J (2015) Hierarchical multiview rigid registration (2015) Comput Graph Forum. (34), 77-87.
[19] Franklin D, Cardini A, Flavel A, Kuliukas A (2013) Estimation of sex from cranial measurements in a Western Australian population. Forensic Sci Int 232(1-3), 153-153.
[20] Dias P, Neves L, Santos D, Coelho C, Ferreira MT, Santos H, Silva S, Santos BS (2015) CraMs: Craniometric Analysis Application Using 3D Skull Models. IEEE Comput Graph Appl 35(6), 11-17.
[21] Mydlová M, Dupej J, Koudelová J, Velemínská J (2015) Sexual dimorphism of facial appearance in ageing human adults: A cross-sectional study. Forensic Sci Int 257, 519.e1-519.e9.
[22] Ramsthaler, F., Kreutz, K., Verhoff, M.A., 2007. Accuracy of metric sex analysis of skeletal remains using Fordisc® based on a recent skull collection. INT J Legal Med 121(6), 477-482.
[23] Torimitsu, S., Makino, Y., Saitoh, H., Sakuma, A., Ishii, N., Yajima, D., Inokuchi, G., Motomura, A., Chiba, F., Yamaguchi, R., 2015. Morphometric analysis of sex differences in contemporary Japanese pelves using multidetector computed tomography. Forensic Sci Int 257, 530.e1-530.e7.
[24] Spradley MK, Jantz RL (2015) Sex estimation in forensic anthropology: skull versus postcranial elements. J Forensic Sci 56(2), 289-296.

[25] Dong H, Deng M, Wang W, Zhang J, Mu J, Zhu G (2015) Sexual dimorphism of the mandible in a contemporary Chinese Han population. Forensic Sci Int 255, 9-15.
[26] Claes P, Walters M, Shriver MD, Puts D, Gibson G, Clement J, Baynam G, Verbeke G, Vandermeulen D, Suetens P (2012) Sexual dimorphism in multiple aspects of 3D facial symmetry and asymmetry defined by spatially dense geometric morphometrics. J Anat 221(2), 97-114.
[27] Shui W, Zhou M, Maddock S, He T, Wang X, Deng Q (2017) A PCA-Based method for determining craniofacial relationship and sexual dimorphism of facial shapes. Comput Biol Med 90, 33-49.
[28] Mitteroecker P, Gunz P, Windhager S, Schaeferc K (2013) A brief review of shape, form, and allometry in geometric morphometrics, with applications to human facial morphology. Hystrix, the Italian Journal of Mammalogy, 24(1), 59-66.
[29] Blanz V, VetterT (1999) A morphable model for the synthesis of 3D faces. In Proceedings of ACM SIGGRAPH 99, 187-194.
[30]Velemínská J, Bigoni L, Krajíček V, Borskýb J, Šmahelováa D, Cagáňováa V, Peterkaad M (2012) Surface facial modelling and allometry in relation to sexual dimorphism. HOMO-Journal of Comparative Human Biology 63, 81-93.
[31] Hu Y, Yin, Duan F, Yin B, Zhou M, Sun Y, Wu Z, Geng G(2013) A hierarchical dense deformable model for 3d face reconstruction from skull. Multimed Tools Appl 64,345-364.
[32] Claes P, Walters M, Clement J(2012) Improved facial outcome assessment using a 3d anthropometric mask. Int J Oral Maxillofac Surg 41, 324-330.
[33] Myronenko A and Song X (2010) Point set registration: Coherent point drift. IEEE Trans Pattern Anal Mach Intell 32(12), 2262-2275.
[34] Amberg B, Romdhani S, Vetter T (2007) Optimal step nonrigid ICP algorithms for surface registration. IEEE Conference on Computer Vision and Pattern Recognition, 1-8.
[35] Booth J, Roussos A, Zafeiriou S, Ponniah A, Dunaway D (2016) A 3D morphable model learnt from 10,000 faces. In Proceedings of the IEEE Conference on Computer Vision and Pattern Recognition, 5543-5552.
[36] Paysan P, Knothe R, Amberg B, Romdhani S, Vetter T (2009) A 3D face model for pose and illumination invariant face recognition. In Proceedings of Sixth IEEE International Conference on Advanced Video and Signal Based Surveillance, 296-301.
[37] Booth J, Roussos A, Ponniah A, Dunaway D, Zafeiriou S (2018) Large scale 3D morphable models. Int J Comput Vis 126, 233-254.
[38] Duan F, Yang S, Huang D, Hu Y,Wu Z, Zhou M (2014) Craniofacial reconstruction based on multi-linear subspace analysis. Multimed Tools Appl 73, 809-823.
[39] Berar M, Tilotta FM, Glaunès JA, Rozenholc Y (2011) Craniofacial reconstruction as a prediction problem using a Latent Root Regression model. Forensic Sci Int 210, 228-236.
[40] Duan F, Huang D, Tian Y, Lu K, Wu Z, Zhou M (2015) 3D face reconstruction from skull by regression modeling in shape parameter spaces. Neurocomputing 151, 674-682.
[41] Deng Q, Zhou M, Wu Z, Shui W, Ji Y, Wang X, Liu CY, Huang Y, Jiang H (2016) A regional method for craniofacial reconstruction based on coordinate adjustments and a new fusion strategy. Forensic Sci Int 259, 19-31.
[42] Chakravarty MM, Aleong R, Leonard G, Perron M, Pike GB, Richer L, Veillette S, Pausova Z, Paus T (2011) Automated analysis of craniofacial morphology using magnetic resonance images. PloS one 6, e20241.

[43] Lorensen WE, Cline HE (1987) Marching cubes: A high resolution 3D surface construction algorithm. ACM T Graphic 21(4), 163-169.
[44] Shui W, Zhou M, Deng Q, Wu Z, Ji Y, Li K, He T, Jiang H (2016) Densely Calculated Facial Soft Tissue Thickness for Craniofacial Reconstruction in Chinese Adults. Forensic Sci Int 266, 573.e1-573.e12.
[45] Aiger D, Mitra NJ, Cohen-Or D (2008) 4-points congruent sets for robust pairwise surface registration. ACM T Graphic 27(3), No.85.
[46] Brown BJ, Rusinkiewicz S (2007) Global non-rigid alignment of 3-D scans. ACM T Graphic 26(3), No.21.
[47] Tai CL, Hu SM, Huang QX (2003) Approximate merging of B-spline curves via knot adjustment and constrained optimization. Comput Aided Des 35(10), 893-899.
[48] Shui W, Zhou M, Ji Y, Yin R (2013) Facial soft Tissue Thickness Measurement and Its Application in Craniofacial Reconstruction (in Chinese). ACTA Anthropological Sinica32(8),345-353.
[49] Mitteroecker P, Gunz P (2009) Advances in geometric morphometrics. Evolutionary Biology, 36(2), 235-247.
[50] Chang CC, Lin CJ (2011) LIBSVM: a library for support vector machines. ACM Trans Intell Syst Technol 2(3) 2, No.27.
[51] Frowd CD, Hancock PJ, Carson D (2004) EvoFIT: A holistic, evolutionary facial imaging technique for creating composites. ACM Trans Appl Percept, 1(1), 19-39.
[42] Hancock PJ (2000) Evolving faces from principal components. Behavior Research Methods, Instruments & Computers, 32(2), 327-333.
[53] Shui W, Zhou M, Wu Z, Deng Q (2011) An Approach of Craniofacial Reconstruction Based on Registration (in Chinese). Journal of Computer-Aided Design & Computer Graphics 23(4), 607-614.
[54] Dias P, Santos D, Souza D, Santos H, Coelho C, Ferreira MT, Cunha E, Santos BS (2013) A New Approach for 3D Craniometric Measurements Using 3D Skull Models. Proc. 17th Int'l Conf. Information Visualization (IV), 462-467.
[55] Pei Y, Zha H, Yuan Z (2010) The craniofacial reconstruction from the local structural diversity of skulls. Comput Graph Forum 27: 1711-1718.
[56] Luo L, Wang M, Tian Y, Duan F, Wu Z, Zhou M, Rozenholc Y (2013) Automatic sex determination of skulls based on a statistical shape model. Comput Math Methods Med. No.251628.
[57] Zheng J, Ni S, Wang Y, Zhang B, Teng Y, Jiang S (2018) Sex determination of Han adults in Northeast China using cone beam computer tomography. Forensic Sci Int, 289, 450.e1-450.e7.

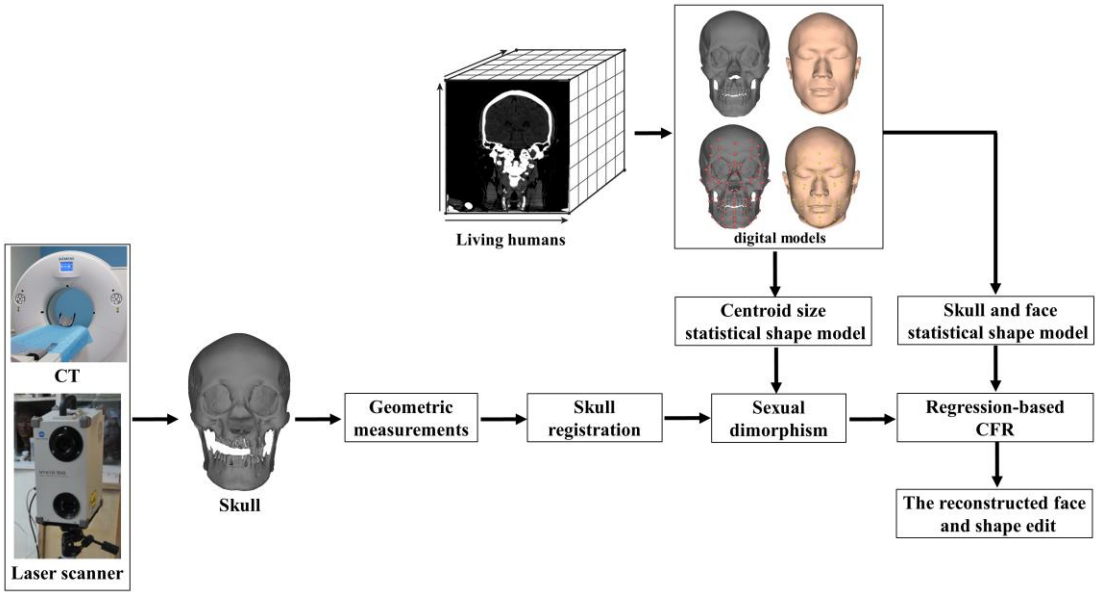

Fig. 1 The technique pipeline of computerized CFR method

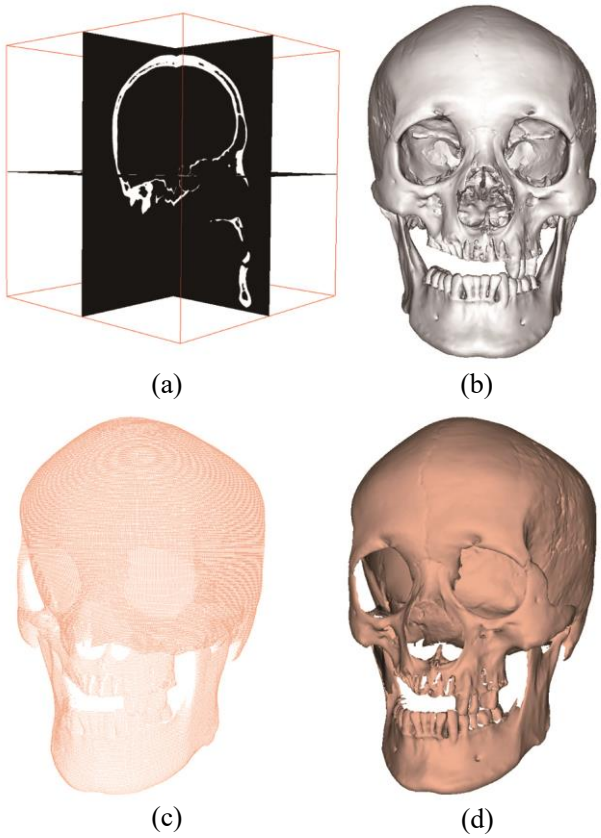

Fig. 2 Skull digitisation using CT images. (a) CT images of the unidentified skull. (b) Digital skull. (c) Exterior point cloud of the unidentified skull. (d) Exterior surface of the unidentified skull.

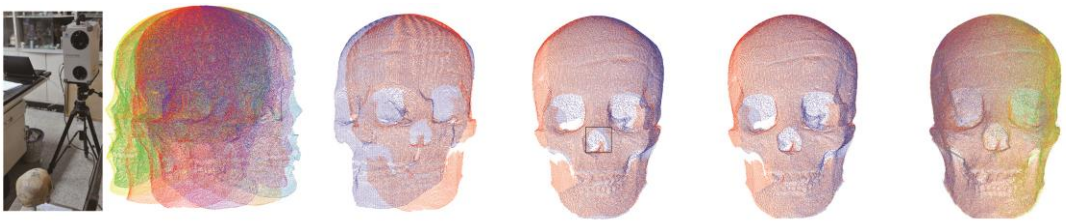

(a) (b) (c) (d) (e)

Fig. 3 Multiple scans acquisition using the VIVID 910. (a) A total of 12 scans. (b) Two neighbouring scans. (c) Coarse registration via the 4PCS algorithm. (d) Fine registration via the ICP algorithm. (e) Global registration.

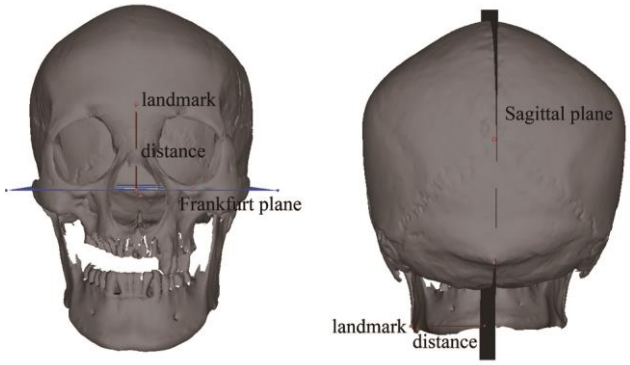

(a) (b)

Fig. 4 Geometric measurement. (a) The distance between the glabella and Frankfurt plane. (b) The distance between the gonion and the sagittal plane.

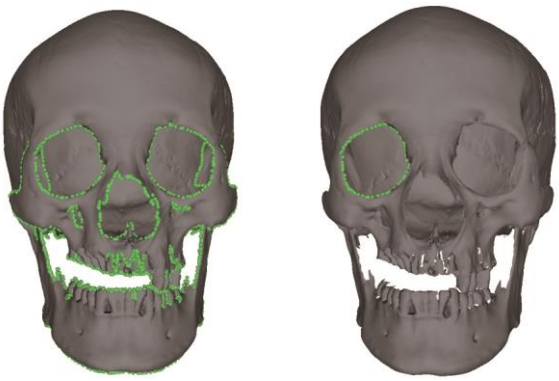

(a) (b)

Fig. 5 Orbital detection and measurements. (a) All boundary curves of the digital skull. (b) Boundary curve extraction.

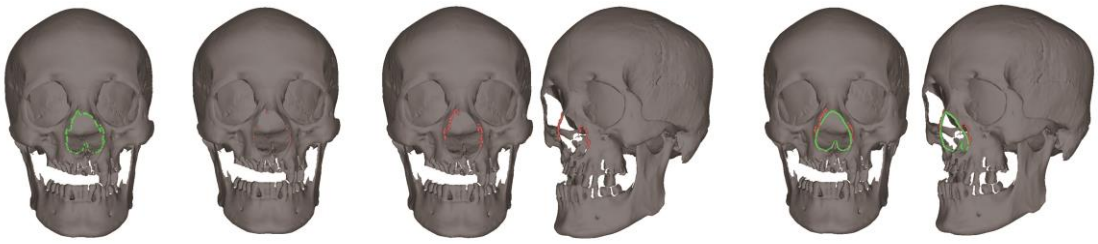

(a) (b) (c) (d)

Fig. 6 Boundary detection of nasal bone and the calculation of the length. (a) Boundary curve extraction (green points). (b) Six points at the start and end of the boundary curve (red points). (c)

Boundary curve vertices of the missing regions (red points). (d) Boundary curve fitting (green points) by deBoor's algorithm.

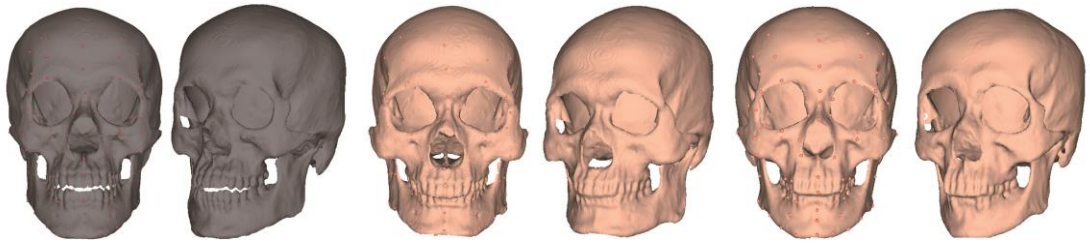

(a) (b) (c)

Fig. 7. The front and profile views of the unidentified skull (grey colour) and two candidate skulls (skin colour). (a) 022 skull. (b) 023 skull. (c) 1231 skull.

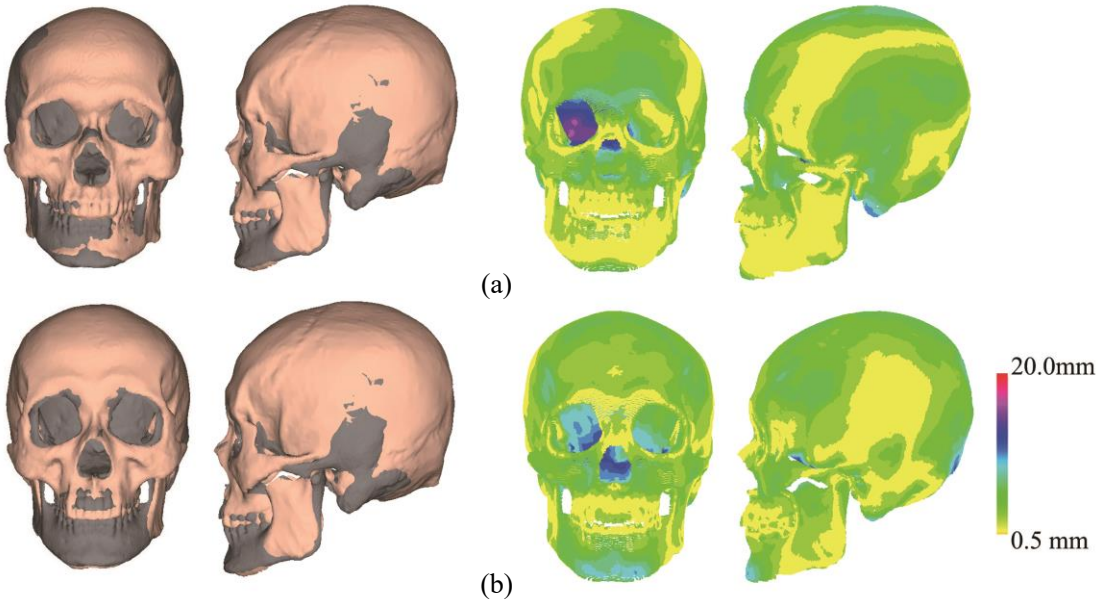

(a)

(b)

Fig. 8. The selection of template skull. From left to right, each image respectively shows the front and profile views of two skulls after ICP registration, and geometric deviation of every vertex between two skulls. (a) Registration result between 023 skull and the unidentified skull. (b) Registration result between 1231 skull and the unidentified skull.

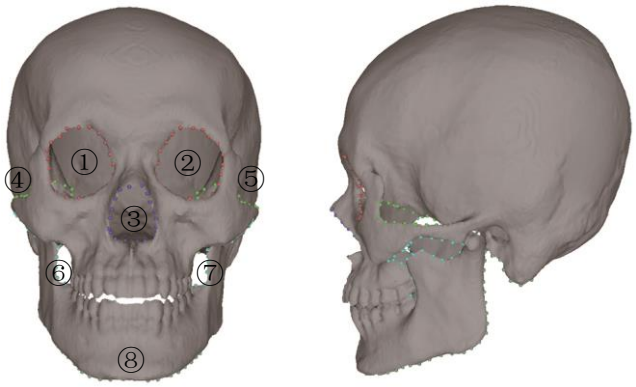

Fig. 9. Eight boundary curves of the skull.

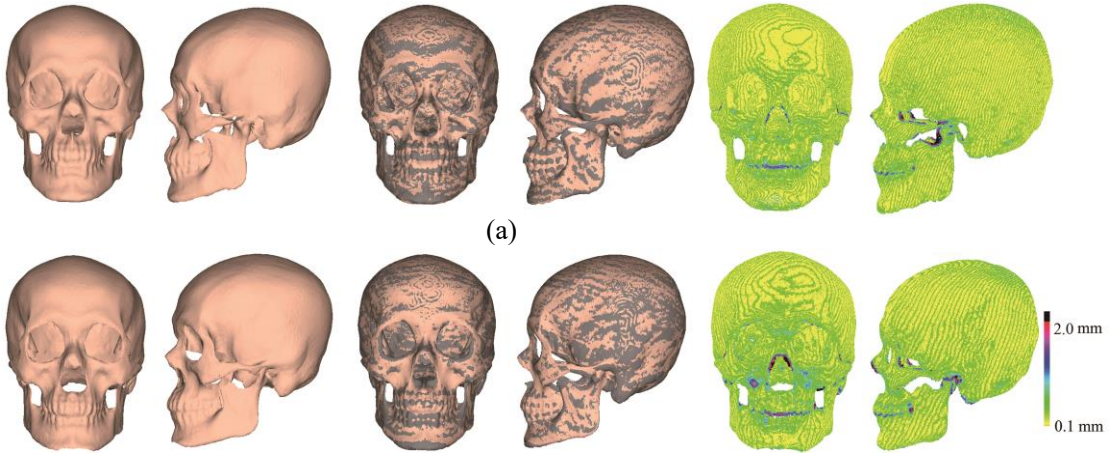

(a) (b)

Fig. 10. The registration results using our method. From left to right, each image respectively shows registration result, registration result (skin colour) and the unidentified skull (grey colour) in the common coordinate system, and registration errors. (a) 1231 skull used as the template model. (b) 023 skull used as the template model.

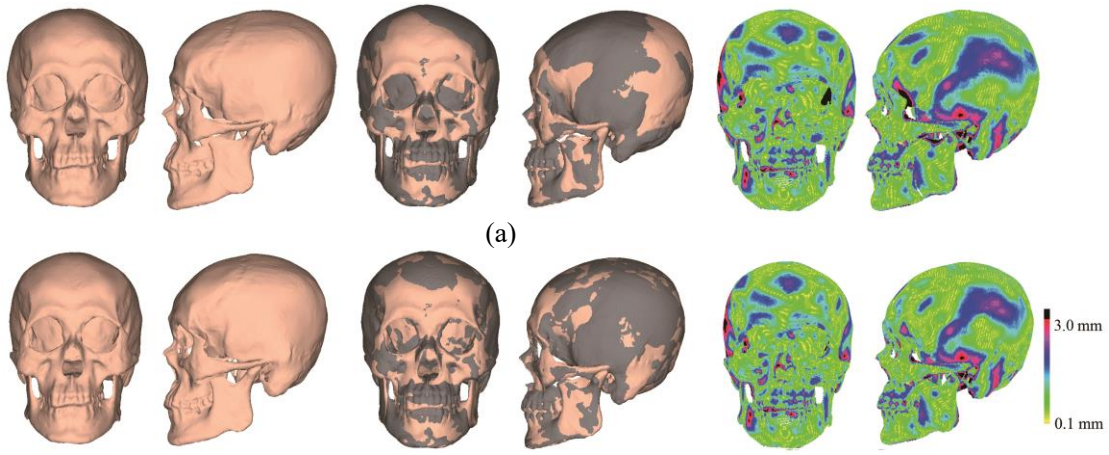

(a) (b)

Fig. 11. The registration results using various registration methods. From left to right, each image respectively shows registration result, registration result (skin colour) and the unidentified skull (grey colour). (a) Registration result using ICP and TPS method [31]. (b) Registration result using TPS and CSRBF method [12].

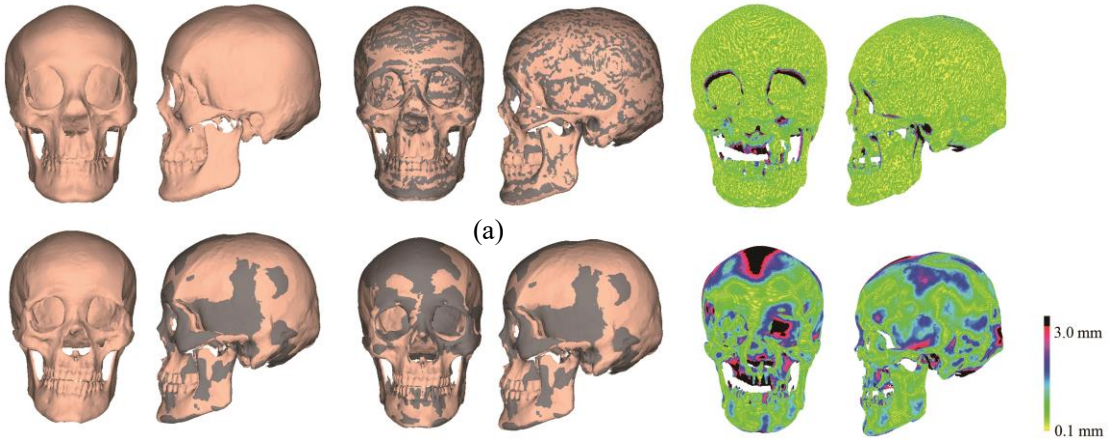

(a)

(b)

Fig. 12. The damaged skull completion. From left to right, each image respectively shows registration result, registration result (skin colour) and the unidentified skull (grey colour) in the common coordinate system, and registration errors. (a) Registration result using our method. (b) Registration result using TPS and CSRBF method [12].

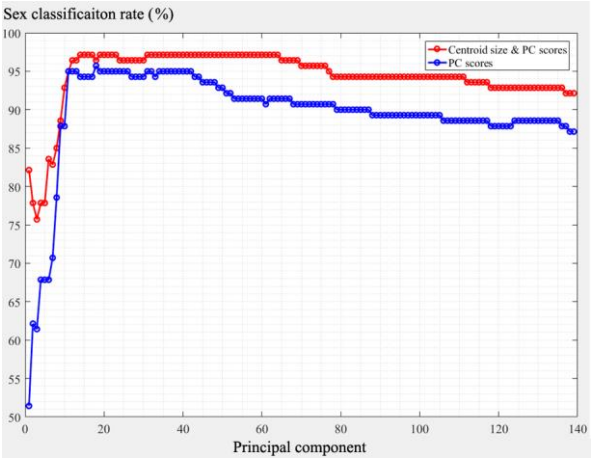

Fig.13 A comparison of sex classification using two methods.

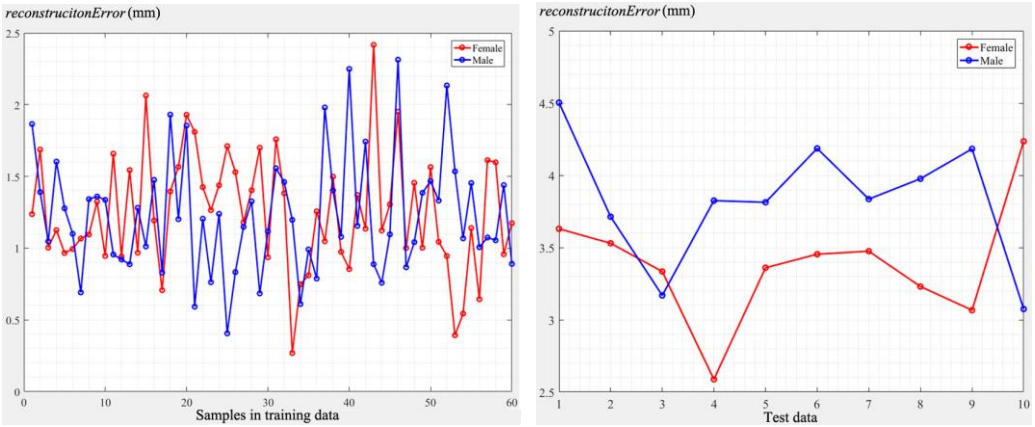

(a) (b)

Fig. 14 Geometric deviation between the reconstructed face and the actual face produced by PC scores and PCs. (a) *reconstructionError* of every sample in the training data. (a) *reconstructionError* of every sample in the test data.

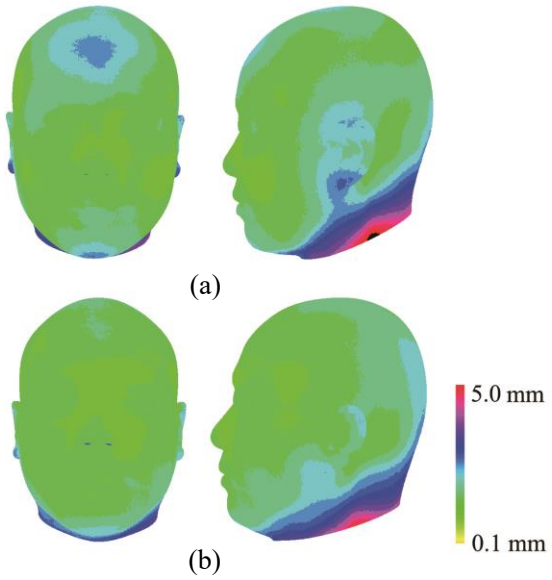

Fig. 15 Visualization of geometric deviation of every vertex between the reconstructed face and the actual face in the training data. (a) Female. (b) Male.

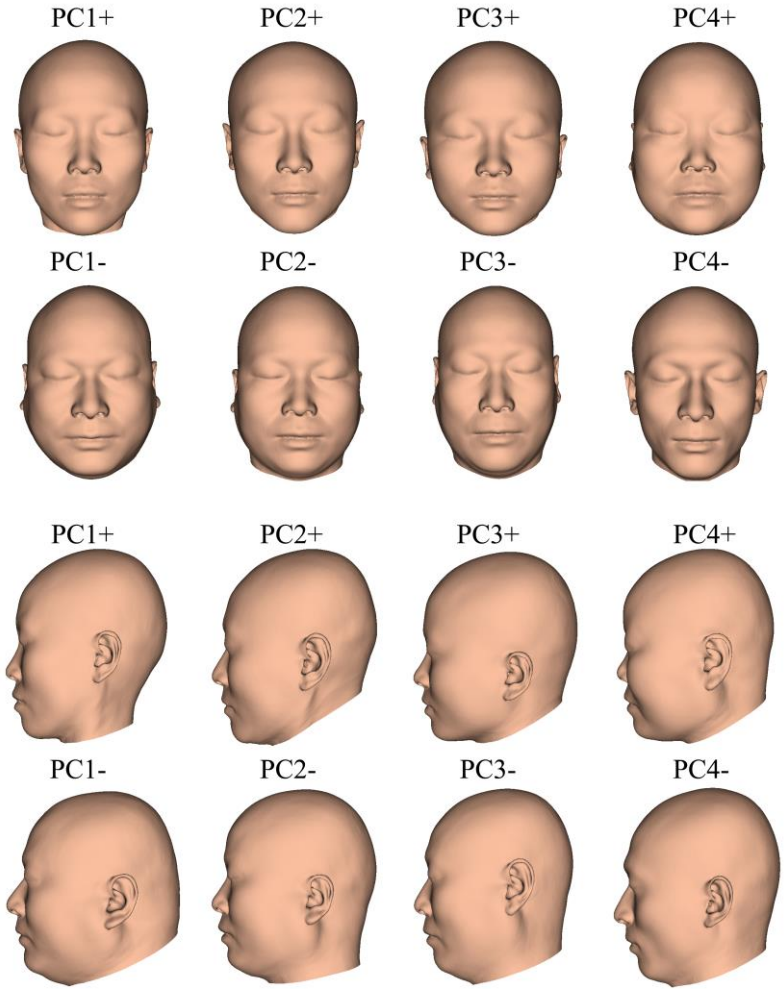

Fig.16 Facial shape variation of all the samples in the first four single PC. Each face is represented by the average face and the *i-th* PC, covering ±3 standard deviations of shape.

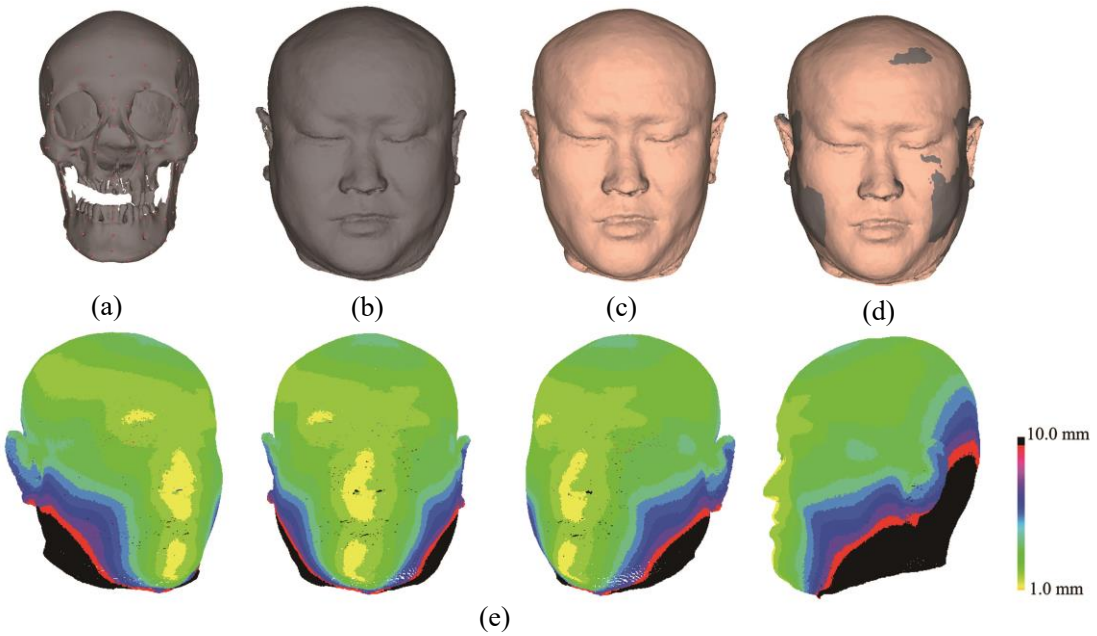

Fig. 17 A computerized CFR example of the damaged skull. (a) The damaged skull. (b) The original reconstructed face. (c) An edited face produced by adjusting PC scores of both PC1 and PC2. (d) The reconstructed face and the edited face located in the common coordinate system. (e) Visualization of geometric difference of every vertex between the reconstructed face and the edited face from various views.